Two-dimensional infrared spectral signature and hydration of the oxalate dianion

Daniel G. Kuroda and Robin M. Hochstrasser[a)]
Department of Chemistry, University of Pennsylvania, Philadelphia, Pennsylvania 19104, USA

(Received 3 August 2011; accepted 17 October 2011; published online 23 November 2011)

Ultrafast vibrational spectra of the aqueous oxalate ion in the region of its carboxylate asymmetric stretch modes show novel relaxation processes. Two-dimensional infrared vibrational echo spectra and the vibrational dynamics obtained from them along with measurements of the anisotropy decay provide a picture in which the localization of the oxalate vibrational excitation onto the carboxylate groups occurs in ∼450 fs. Molecular dynamics simulations are used to characterize the vibrational dynamics in terms of dihedral angle motion between the two carboxylate planes and solvation dynamics. The localization of the oxalate vibrational excitation onto the carboxylates is induced by the fluctuations in the carboxylate vibrational frequencies which are shown by theory and experiment to have a similar correlation time as the anisotropy decay. © *2011 American Institute of Physics*. [doi:10.1063/1.3658461]

I. INTRODUCTION

The determination of the structural and dynamical characteristics of the solvation shells of aqueous ions remains as a challenging area of physical chemistry experimental and theoretical research.[1] The interaction of molecular ions, particularly carboxylates, and water molecules is of great interest in a wide range biological systems. It is well known that water stabilizes molecular ions by forming associated hydrogen bond networks in which water dipoles are oriented toward the ion. The resulting structure and its dynamics alter the properties of both the ion and the surrounding water. Some ions cause the surrounding water to acquire properties that are quite different from those of the bulk solvent.[2,3] In turn, the molecular structures of ions in solution can considerably be modified from those in the gas phase. The sensitivity and time resolution of vibrational spectroscopy has resulted in it becoming the method of choice to study rapid dynamical processes in water.[4–7] Notwithstanding the successes of transient vibration spectra in characterizing the hydration shell dynamics, only a few experiments have focused directly on accessing the vibrational states of the ion to probe the solvation structure and examining the effect of water on the structure and states of the molecular ion.[5,7] If the ion structure is polar, the effects of hydration are difficult to characterize because of the complexity of the low symmetry water shell. So, we have developed the idea of using molecular ions having high enough symmetry to support degenerate states.[6,7] In such cases, the motions of the solvent will lower the ion symmetry and give rise to splitting of the degenerate vibrational states. This splitting and the properties of the resulting eigenstates can provide direct information of the solvent shell structure and dynamics that may not be so obvious from similar experiments on lower symmetry ions. Thus, the present study focuses on understanding the structural and hydration dynamics of the oxalate dianion which is a simple and highly symmetric molecular ion.

Oxalate has two apposed carboxylate groups spaced within a few angstroms (Figure 1). In the gas phase, the symmetry of oxalate is D_{2d} in which the two carboxylate groups form perpendicular planes as represented in Figure 1.[8] In this conformation, the ion has three degenerate vibrational modes. Previous studies indicate definitively that the symmetric and antisymmetric stretch modes of the carboxylate groups of oxalate are to be found in the ranges 1400–1500 cm^{-1} and 1500–1700 cm^{-1}, respectively.[8–10] The oxalate ion is, therefore, expected to have two transitions in each of these regions. However, elementary symmetry arguments lead to the conclusion that only the antisymmetric combination of carboxylate symmetric stretches has a dipole derivative and is allowed in the infrared (IR). Thus, only one transition is expected to be observable in the symmetric stretch region of the infrared spectrum regardless of the dihedral angle between the two carboxylate planes. The asymmetric stretch vibration of carboxylate (Figure 1) is near 1575 cm^{-1}.[8] The situation in this asymmetric stretch region of oxalate is more complex than for the symmetric stretch since its frequency position depends on whether or not the carboxylate planes are parallel. If they are parallel (dihedral angle zero, D_{2h} symmetry), then only one of the two asymmetric stretch components is IR allowed. If not, there should be two allowed transitions having frequencies and absorption cross sections that depend on the dihedral angle. However, when the dihedral angle is 90°, these two frequencies and cross sections become equal, the modes become the components of the degenerate E mode of the D_{2d} symmetry molecule, and only one band is expected in the antisymmetric stretch region. In contrast to oxalate's conformation in the crystalline phase,[11] the gas phase structure[12] shows a dihedral angle of 90°, and it will be shown below that this is the most likely structure of oxalate in water.

The short distance of 1.5 Å between the charged centers in oxalate not only defines the dianion structure, but also

a)Electronic mail: hochstra@sas.upenn.edu.

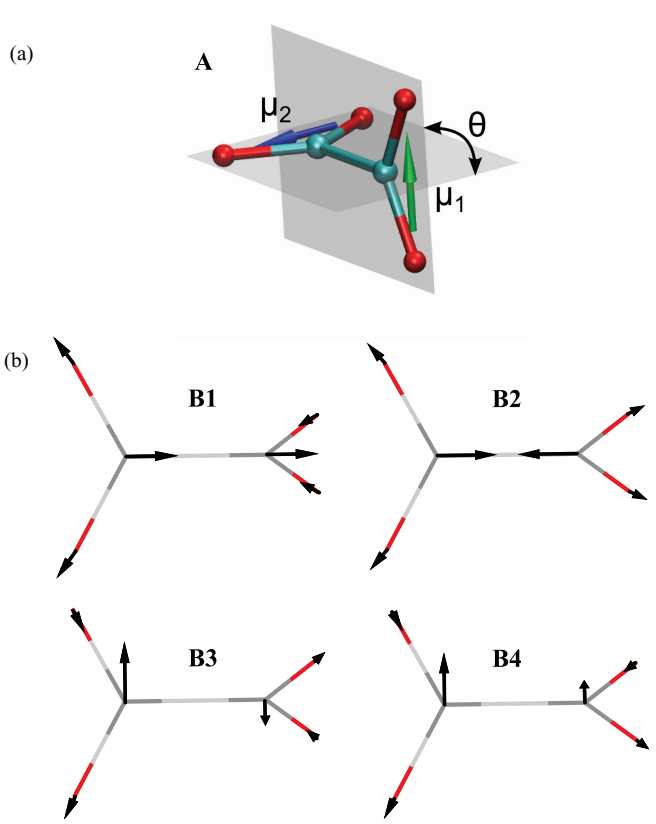

FIG. 1. Oxalate geometry and vibrational modes. (a) Oxalate equilibrium conformation. Green and blue arrows represent the transition dipole moment direction for each carboxylate asymmetric stretch. (b) Symmetric (b1, b2) and asymmetric (b3, b4) stretch vibrational modes. The atomic displacements are indicated with black arrows.

creates a situation where the hydration shells of the two carboxylates are not simply separable. Thus, the conformation of oxalate is a compromise between the interaction between the two carboxylate groups and their coupling with water molecules in the hydration shell. On the one hand, the carboxylates try to minimize the Coulombic repulsion by adopting a 90° conformation, whereas the strong association with water molecules in the same solvation shell can disrupt this spatial arrangement to favor oxalate dihedral angles that better fit with the water network. Interestingly, the potential energy for internal rotation of the dihedral angle is sufficiently shallow that at room temperature the oxalate dihedral can regularly be found away from its 90° minimum. Moreover, the thermal fluctuations of oxalate's dihedral angle disrupt the degeneracy of the asymmetric stretch and create a system of two separated but coupled nondegenerate states. In addition, solvent fluctuations around each carboxylate at a nearly fixed oxalate conformation can also induce a lowering of the symmetry and a splitting of the degeneracy. This delicate equilibrium among structure, solvation, and vibrational dynamics presents new questions regarding the role of water on molecular ion structure. Time-resolved vibrational spectroscopy is an ideal tool to investigate solvation shell and conformation dynamics. In particular, two-dimensional (2D) IR has the uniqueness of providing direct insights into processes such as transition dipole reorientational motions, intermode coupling, and time-dependent frequencies for system with nearly degenerate or degenerate transitions.[6,7,13,14] Moreover, 2D IR is a well-established technique for studying the solvation shell dynamics.[5,15,16]

The aim of this paper is to explore the vibrational and conformational changes of oxalate in aqueous solution by probing the asymmetric stretch of oxalate at ~1575 cm^{-1} with ultrafast time resolution. For this purpose, femtosecond IR pump-probe and 2D IR in conjunction with linear FTIR spectroscopy are employed. In addition, molecular dynamics (MD) simulations are used to obtain the time evolution of the density matrix for the pair of carboxylates and a density functional theory (DFT) frequency map is analyzed and modeled to shed light on the conformational, hydration, and vibrational dynamics of oxalate.

II. MATERIALS AND METHODS

A. Sample preparation

Sodium oxalate ($C_2O_4Na_2$, >99%), cesium oxalate ($C_2O_4Cs_2$, >99%), and its isotopologue ($^{13}C_2O_4Na_2$, 99% atom ^{13}C) were obtained from Sigma Aldrich and deuterium oxide (D_2O, 100.0 atom% D) from Acros Organics. All chemicals were used without further purification. The solutes were dissolved in D_2O to obtain a concentration of 0.10 M. Room temperature (25 °C) was used in all experiments.

B. Infrared spectroscopies

The FTIR absorption spectra were acquired with a Thermo Nicolet 6700 spectrometer having 0.5 cm^{-1} resolution in sample cells with CaF_2 windows and a 6 μm path length.

The 2D IR spectra were collected by heterodyned spectral interferometry and processed according to the previously described techniques.[17] A Ti:Sapphire amplifier is used to generate infrared Fourier transform limited pulses in a homemade optical parametric amplifier (OPA) coupled with a difference frequency generator. The IR source consisting of 80 fs duration pulses centered at 1580 cm^{-1} is divided into three replicas (wave-vectors: $\mathbf{k}_1$, $\mathbf{k}_2$, and $\mathbf{k}_3$) and focused at the sample using the box configuration geometry. The photon echo signal due to the interaction of the sample with the IR pulses is produced and detected in the $-\mathbf{k}_1 + \mathbf{k}_2 + \mathbf{k}_3$ phase matching direction by heterodyning it with a fourth IR pulse (LO) after dispersion by a monochromator (50 grooves/mm) and detected with a 64 element HgCdTe array detector. In all the experiments, the signal field was measured by combining it on the array detector with the dispersed LO pulse that precedes it by 1 ps. Two time sequences of pulses, each with a set of specific polarizations of the IR pulses, were used to obtain the corresponding two-dimensional spectra. The sequence where the pulses with the wave vector $\mathbf{k}_1$ arrive at the sample before those with wave vector $\mathbf{k}_2$ produces the rephasing echo signals. The nonrephasing spectrum is generated with a time inverted sequence of pulses, i.e., $\mathbf{k}_2$ arrives before $\mathbf{k}_1$. In both sequences, the coherence time interval τ

between $\mathbf{k}_1$ and $\mathbf{k}_2$ was scanned with a 2 fs step. The time dependence of the photon echo with the population time T, time interval between second and third pulses, was produced by scanning the third pulse $\mathbf{k_3}$ with 200 fs steps from 0 to 2 ps. The two-dimensional spectrum obtained by Fourier transformation of the signal measures the correlation between the frequencies ω_τ and ω_t of the coherences that evolve during the τ and t intervals. A detailed explanation of the two-dimensional analysis can be found in Ref. 17.

The pump-probe spectra were collected using the previously described setup[4,6] The experimental setup included a femtosecond regenerative amplifier (Spitfire, Spectra Physics) to generate a tunable mid-infrared output from a homemade OPA. The infrared source delivers nearly transformed limited pulses (∼75 fs duration, 250 cm^{-1} FWHM) centered at ∼6 μm with energies of 2.4 μJ which are split into pump and probe pulses. The pump energy at the sample was ∼500 nJ and the probe is attenuated to an energy at least ten times lower than this. The pulses are focused to a spot size of less than 200 μm in the sample. The probe beam is detected on a spectrometer with a 100 grooves/mm grating and a 32-element HgCdTe array detector. The delay between pump-probe is controlled with a motorized translation stage. In this work, the population lifetimes were measured by detecting the probe polarization at the magic angle with respect to the pump. The time dependent anisotropy measurements were carried out by detecting the probe polarization components parallel (I_{ZZ}) and perpendicular (I_{ZX}) to the pump, with the incident probe polarization set at 45° to that of the pump.

C. Simulation method

The molecular dynamics simulations were performed using the SANDER module of the AMBER 9 program package.[18] A quantum mechanical molecular dynamics method was used to describe the oxalate force field. The oxalate ion structure was parameterized according to parameterized model number 3 (PM3) semi-empirical formalism and water was modeled classically with the transferable intermolecular potential 3P (TIP3P) force field. The system consisted of the ion embedded in 35 Å cube containing ∼1400 water molecules. Periodic boundary conditions were imposed in the simulation. Particle-mesh Ewald methodology was used for long-range electrostatic interactions with a cutoff of 12 Å. The SHAKE algorithm was used to fix the bonds involving hydrogen. The simulation was initiated using an initial geometry for oxalate obtained from the *ab initio* DFT calculations performed at the B3LYP/6-31+G** levels using the GAUSSIAN 03 and 09 software packages.

The system was energy-minimized for 200 steps using the steepest descent method followed by 300 steps with the conjugate gradient method. Subsequently, the system was equilibrated at a normal pressure and temperature (*NPT*) for 1 ns with a 2 fs step. Finally, a production run at *NPT* was recorded for 5 ns extracting snapshots every 4 fs. All simulations used a Langevin thermostat for temperature control.

D. Potential of mean force

The potential of mean force in water for the variation of the dihedral angle between the two carboxylate planes was calculated by means of the umbrella sampling MD simulations combined with the weighted histogram analysis method (WHAM).[19] Thirty-seven separate MD runs, each having a 5° window, were sampled for 0.5 ns to cover the −90° to 270° rotational coordinate of oxalate. A harmonic biasing potential of 0.02 kcal/(mol. deg^2) was applied as umbrella. Except for the harmonic constraint, all simulation parameters used were the same as those used in the MD simulations.

E. Carboxylate frequency fluctuations

We used a DFT map developed for the acetate ion[20] to simulate the frequency fluctuations of each of the carboxylate asymmetric stretching modes in oxalate. The DFT map provides the correlation of the asymmetric stretch frequency with electric fields and their gradients at the C, O_1, and O_2 atoms. This map shows a good correlation between the electric field and DFT frequencies for 33 electrostatic parameters, five of which correspond to components of electric fields at these atoms and the remainder to electric field gradients at the same points. The linear infrared spectrum estimated with this map exhibited a good agreement with experiments on carboxylate.[5]

III. RESULTS

The FTIR spectrum of the oxalate anion in a D_2O solution shows two bands at frequencies higher than 1200 cm^{-1}. The carboxylate symmetric stretch band of $^{12}C_2O_4^{2-}$ located at 1312 cm^{-1} has a symmetric band shape and a peak extinction coefficient of 1830 $M^{-1}cm^{-1}$. The antisymmetric stretch transition observed at 1579 cm^{-1} is a distinctly asymmetric absorption band which is broadened on the high frequency side (Figure 2). This 1579 cm^{-1} band has a peak extinction of 2380 M^{-1} cm^{-1} and has extinction coefficient of 105 700 $M^{-1}cm^{-2}$ that is twice that of the asymmetric stretch transition of trifluoroacetate (TFA). The $^{13}C_2O_4^{2-}$ isotopologue also shows two transitions above 1200 cm^{-1} which are down shifted by 37 cm^{-1} (symmetric stretch) and 43 cm^{-1} (asymmetric stretch) with respect to the $^{12}C_2O_4^{2-}$ transitions. Figure 2 shows the infrared spectra for both isotopologues with solvent D_2O background subtracted. Although the $^{12}C_2O_4^{2-}$ and $^{13}C_2O_4^{2-}$ isotopologues have different carboxylate asymmetric and symmetric stretch transition frequencies, the spectral shapes and widths of the bands are not significantly isotope dependent. Furthermore 1:1 molar mixture of the isotopologues $^{12}C_2O_4^{2-}$ and $^{13}C_2O_4^{2-}$ has an FTIR spectrum (not shown) that is equal to the sum of the individual spectral components consistent with the absence of any aggregation.

The small shoulder present at the high frequency side of the asymmetric stretch band (Figure 2) is attributed to species involving ion pairs. It is well known that doubly charged ions may associate with the counter ions to form ion pairs which have shifted vibrational frequencies.[21] The interesting topics

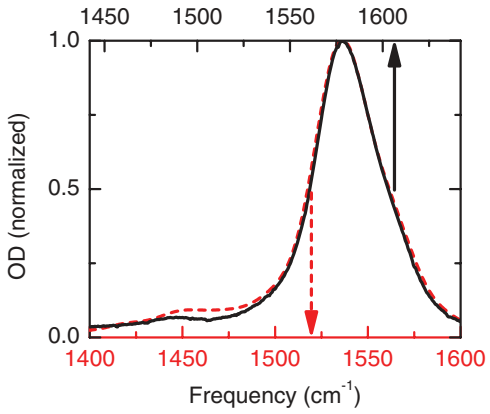

FIG. 2. Experimental linear IR spectra. $^{12}C_2O_4^{2-}$ (solid line, upper scale) and $^{13}C_2O_4^{2-}$ (red dashed line, lower scale) in D_2O.

of ion pair formation and ion pair frequencies are not the main focus of this work and will be fully analyzed in a subsequent report.

The transient spectral response of $^{12}C_2O_4^{2-}$ in D_2O produced by a pump pulse centered at 1575 cm^{-1} is shown in Figure 3. Both the photo-induced and bleach signals show the same dynamics within the signal-to-noise of the experiment.[22] The dynamics of the photo induced signal is reproduced by the sum of two exponentials. The time constants (normalized amplitudes) of the new absorption band are 0.3 ps (0.7) and 1.6 ps (0.3), respectively. Also, the new absorption signals $S_{\parallel}$ and $S_{\perp}$ yield a fast anisotropy decay $r(t)$ that it is well described by the function:

$$r(t) = Ae^{-t/\tau} + B, \tag{1}$$

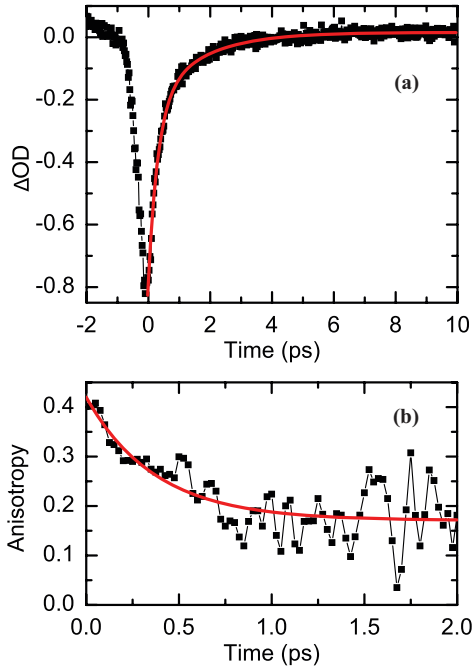

FIG. 3. Pump-probe dynamics of oxalate at 1550 cm^{-1}. (a) Photo-induced transient signal (black filled squares) and biexponential fit (red line). (b) Anisotropy signal (black filled squares) and exponential fit (red line).

which is characterized by a decay time constant of $\tau = 0.4 \pm 0.1$ ps and amplitudes $B = 0.16 \pm 0.02$ (error 1 standard deviation) and $A + B = 0.4$ within experimental error.

The 2D-IR spectra of aqueous oxalate was also investigated at different waiting times (Figure 4). At T = 0 the asymmetric stretch transition is distinctly elongated along the diagonal both for the positive $v = 0 \rightarrow 1$ transition contribution and the negative $v = 1 \rightarrow 2$ region. At the shortest waiting times where reliable 2D IR spectra could be obtained from the unrelaxed inhomogeneous distribution, the better resolved spectra (Figure 4) appear to be composed of at least three transitions. The background D_2O signal was negligible in all these experiments.

At later waiting times, these initially elongated peaks reshape to expose more clearly three different transitions located at 1562 cm^{-1}, 1585 cm^{-1}, and 1608 cm^{-1}. The central, strongest transition ($\omega_\tau = \omega_t = 1585$ cm^{-1}) has a significant elongation along the diagonal of the ω_τ, ω_t plot at T = 0 (Figure 4). At later waiting times (T > 2 ps), this central part of the spectrum acquires a fully upright shape aligned with the frequency axes instead of the diagonal line. This change in shape is a manifestation of the spectral diffusion of the oscillator and the resulting loss of correlation between the pumped and probed coherences. The highest and lowest frequency transitions ($\omega_\tau = \omega_t = 1562$ cm^{-1} and 1608 cm^{-1}) become most clearly distinguishable from the remainder of the spectrum at waiting times longer than 400 fs. In contrast to the 1585 cm^{-1} transition, the other two transitions, 1562 cm^{-1} and 1608 cm^{-1}, do not show any significant change in their elongation along the diagonal line, even at large waiting times (T > 2 ps). The spectral features of these two transitions are characteristic of the spectral diffusion being slow on the time scale of the population decay. This result indicates that these transitions most likely evidence the presence of a species other than the free ion. It can be shown that the bands are transitions of the ion pair where the water molecules causing the frequency relaxation of free oxalate have restricted access and modified properties compared with the carboxylates of the ion pair, as will be discussed in more detail below and in a separate publication.

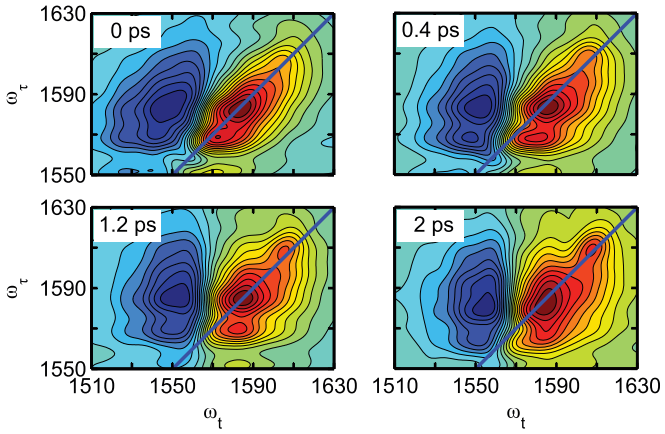

FIG. 4. Experimental 2D IR vibrational echo spectra of oxalate in D_2O for population times T = 0 fs, T = 400 fs, T = 1200 fs, and T = 2000 ps.

IV. DISCUSSION

First a model is introduced for which solution of the time-dependent Schrödinger equation yields the frequency and population dynamics for the pair of asymmetric stretch modes of oxalate. Then, it is shown that the anisotropy of the dianion is rapidly diminished by transitions between the two delocalized states of the dianion. The relative effects of fluctuations in the coupling between the carboxylates due to their motion on the dihedral angle potential of mean force, and the water induced fluctuations of the local vibrational frequencies are then addressed quantitatively.

A. The theoretical model

In order to predict the vibrational spectra and the ultrafast internal motions of the pair of carboxylates in oxalate, a dynamical model is needed that incorporates their time-dependent frequencies and the angular dependent couplings between them.

In the modeling of the dynamical conformation of oxalate, it is assumed that each of the $-CO_2^-$ groups is planar. All the internal vibrations except the dihedral angle coordinate relating the two carboxylate planes are frozen, but the overall rotation is incorporated, albeit in a simplified manner. The internal rotation occurs at a fixed C–C separation of ~1.5 Å (Figure 1). In the electronic ground state of the oxalate ion, internal rotation of the carboxylates groups about the C–C bond is hindered by a potential that favors the structure where the dihedral angle is $\pi/2$. The potential of mean force for the movement of oxalate's dihedral angle is shown in Figure 5. The thermal distribution of angles at 300 K is also shown in Figure 5. The potential energy equals k_BT for angular displacements of $\pm 30^\circ$ from the equilibrium position at 90°. Moreover, as a guide to the inertial motion, the period of small oscillations of the oxalate dihedral angle assuming a harmonic potential around the $\pi/2$ minimum in the potential is 0.8 ps corresponding to a frequency of 42 cm^{-1}. The rotation barrier on the mean force potential at 0 and π is 3.6 Kcal/mol. First the semi-classical Hamiltonian is discussed.

1. The Hamiltonian

The system consists of two carboxylates that are each undergoing vibrational frequency fluctuations in addition to being coupled by a time-varying potential that depends on the dihedral angle. At each instant, the vibrational modes of an oxalate ion are superpositions of the site carboxylate modes. In the internal rotor model for the asymmetric stretch modes, the instantaneous vibrational Hamiltonian of the oxalate's one vibrational quantum eigenstates is represented by

$$H(t) = \begin{bmatrix} \omega'_1(t) & \beta(t) \\ \beta(t) & \omega'_2(t) \end{bmatrix}, \tag{2}$$

where $\beta(t)$ is the time-varying coupling strength between the two carboxylate asymmetric stretch modes and $\omega'_i(t)$ represents the instantaneous $v = 0 \rightarrow v = 1$ vibrational frequency of the ith site carboxylate group, defined as the sum of the unperturbed transition frequency of the site (ω_i) and the site frequency fluctuation due to solvent dynamics ($\delta\omega_i(t)$) but independent of any coupling between sites. The diagonalization of the Hamiltonian (Eq. (2)) leads to the frequencies of the single quantum states and to their corresponding eigenstates which are linear combinations of the site states. The one quantum eigenstates of the Hamiltonian are represented as

$$|\pm(t)\rangle = c_1(t)|1\rangle \pm c_2(t)|2\rangle, \tag{3}$$

where all the $\{c_1(t), c_2(t)\}$ coefficients are the eigenvectors of the diagonal vibrational Hamiltonian.

This vibrational Hamiltonian depends on two processes: the instantaneous frequencies of the sites and the instantaneous coupling. While the frequency deviations are modeled according to the instantaneous solvent coordinates and a DFT map, an exciton model is used to describe the dynamic coupling between the two carboxylate asymmetric stretches. In this exciton model, each of the carboxylate transition dipoles is directed parallel to a line connecting the two oxygen atoms of either carboxylate and they are represented as vectors $\boldsymbol{\mu}_{01}^{(1)} = \boldsymbol{\mu}_{01}\hat{1}$ and $\mu_{01}^{(2)} = \mu_{01}\hat{2}$ located at the centers of mass of the carboxylate groups (Figure 1) where μ_{01} is the transition dipole magnitude for the $v = 0$ to $v = 1$ transition of a single carboxylate asymmetric stretch mode. The unit vectors $\hat{\pm} = (\hat{1}(t) \pm \hat{2}(t))/\sqrt{2}$ are independent of time because the dihedral angle changes only result in changes of the magnitudes of the transition dipoles to the delocalized states which are given at time t as

$$|\mu_{\pm 0}| = \mu_{01}\sqrt{(1 \pm \cos\theta(t))}. \tag{4}$$

The use of such a dipole moment neglects any changes in the site transition moments by inter-carboxylate or solvent interactions. It will be seen that the transition dipole magnitudes in Eq. (4) are essential for the calculation of frequency fluctuations. Since oxalate is modeled as an internal rotor, the site transition dipoles move in planes that are perpendicular to the C–C bond axis and parallel to each other so that at any given instant the energy is defined by one dihedral angle between the $-CO_2^-$ planes. The transition dipole coupling (TDC) between site modes was evaluated using three different models: transition dipole coupling which is not likely to be quantitatively correct for such nearby oscillators but is nevertheless a useful comparison, transition charge coupling (TCC) which should be an improvement on TDC, and DFT

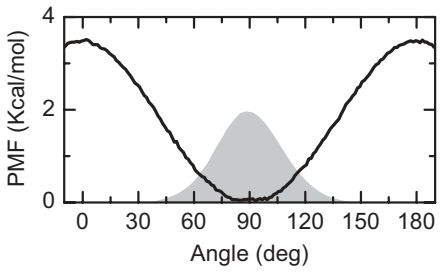

FIG. 5. Potential of mean force computed for oxalate. The shaded area shows the distribution of states at 300 K.

calculations. For the case of TDC, the coupling is obtained for each dihedral with the following formula:

$$\beta = \mu^2 \frac{\cos\theta(t)}{r^3}, \tag{5}$$

where the transition dipole moment $\mu = \mu_{01} = \mu_{02}$, r is the fixed distance between dipoles, and $\theta(t)$ is the angle between them. It should be noted that β adopts a change in sign on either side of $\pi/2$: i.e., $\beta(\pi/2+\phi) = -\beta(\pi/2-\phi)$. In TCC, the coupling constant is expressed as follows:

$$\beta = \frac{1}{2} Q_l Q_m \left[\sum_{a_l b_m} \frac{\partial^2}{\partial Q_l \partial Q_m} \left(\frac{\left(\sum_{n=0}^{2} \frac{q_{a_l}^{(n)}(0)}{n!} (Q_l)^n \right) \left(\sum_{n=0}^{2} \frac{q_{b_m}^{(n)}(0)}{n!} (Q_m)^n \right)}{r_{a_l b_m}} \right) \right]. \tag{6}$$

Here, subscripts a and b correspond to all the atoms that undergo nuclear displacements in each of the carboxylate sites of oxalate. The $q_{a_l}^{(n)}(0)$ denotes the nth derivate of the charge with respect to the dimensionless normal mode coordinate for the lth/mth asymmetric stretch of carboxylate evaluated at equilibrium $Q = 0$, and $r_{a_l b_m}$ is the distance between the indicated atoms. Due to the symmetry of the displacement in the asymmetric stretch coordinate, a second-order Taylor expansion of the charge is needed to accurately model the coupling by TCC. The charges and charge derivatives are obtained from *ab initio* DFT calculations on formate using the same level of theory as in initial geometry of the MD simulation.

The coupling between carboxylate sites using different models is presented in Figure 6. The purely electrostatic interactions TDC and TCC both yield larger couplings than the DFT computation. The TDC appears to significantly overestimate the coupling. While TCC shows a better agreement with DFT calculations, it still gives a significantly larger coupling constant compared with the DFT computation by almost a factor of two. Some of these mismatches between either TDC or TCC and DFT must arise from the non-negligible through bond interaction, since the carboxylates are close enough that they have a significant overlap between electronic densities. Although TCC becomes TDC when the distance between dipoles is large compared to the dipole, both models predict a similar dihedral angular dependence, $\beta \propto \cos\theta$ which is comparable with the angular dependence computed by DFT. The TCC and DFT give quite similar results for the small dihedral angular displacements expected to dominate the thermal distribution at 300 K based on the potential of mean force. However, the main point is that the coupling constant is shown to be well modeled at 300 K with a function of the form $\beta = a\cos\theta$, where a is an empirical factor obtained from fitting of the angular dependence by DFT.

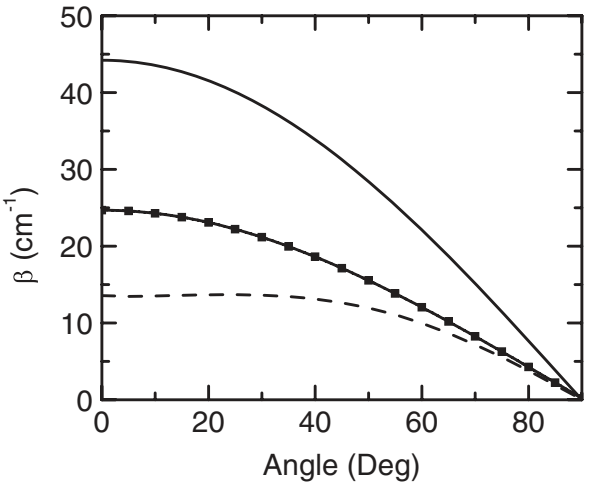

FIG. 6. Coupling constant of oxalates for different levels of theory. The solid, solid with filled squares, and dashed lines represent the coupling constant predicted by TDC, TCC, and DFT, respectively.

To calculate the instantaneous site frequencies ($\omega'_i(t)$), the frequency fluctuation of the asymmetric stretch ($\delta\omega_i(t)$) due to solvent dynamics is computed in each snapshot of the MD simulation by means of the DFT frequency map[20] and electric field parameters.

The linear infrared spectra are calculated using the excitonic frequencies and their corresponding transition dipole lengths obtained by direct diagonalization of the instantaneous Hamiltonian in each step of the MD trajectory. Although the principles of the dynamics of two level systems are well known from Redfield theory,[23] in the present case we use an MD simulation in conjunction with semi-empirical computations to find the relaxation parameters of the oxalate vibrational states. Thus, the vibrational dynamics of the system is determined by solving the time-dependent Schrödinger equation (see below).

a. Linear absorption spectrum. The linear absorption spectrum is obtained from the Fourier transform of the dipole time correlation function as

$$I(\omega) \sim \int_{-\infty}^{\infty} dt e^{-i\omega t} \langle \boldsymbol{\mu}(0) \cdot \hat{\boldsymbol{E}}_l \boldsymbol{\mu}(t) \cdot \hat{\boldsymbol{E}}_l \rangle, \tag{7}$$

where $\boldsymbol{\mu}$ is the dipole operator and $\hat{\boldsymbol{E}}_l$ is the polarization of the electric field. For the ground state to the first excited state transition of a given vibrational mode in an isolated oscillator in the semi-classical limit and assuming that the rotational diffusion describing the overall motion is not correlated with the

changes in the magnitude of the transition dipole and adding the lifetime as an empirical factor, the linear infrared spectrum expression (7) becomes

$$I_1(\omega) \sim \int_{-\infty}^{\infty} e^{-i\omega t} e^{-t/2T_1 - 2Dt} \left\langle \mu_{10}(0)\,\mu_{10}(t) \times \exp\left[i \int_0^t \omega_{10}(\tau)\, d\tau \right] \right\rangle dt, \tag{8}$$

where T_1 is the vibrational population lifetime. To obtain Eq. (8) the system was assumed to have the overall motion of a sphere with rotational diffusion constant D at all dihedral angles. Oxalate has two possible $v = 0 \rightarrow 1$ transitions, which in an exciton picture are $|0\rangle \rightarrow |+\rangle$ and $|0\rangle \rightarrow |-\rangle$. They result in an infrared spectrum that is the sum of contributions from these two transitions:

$$I(\omega) = I_+(\omega) + I_-(\omega). \tag{9}$$

The statistical average in Eq. (8), necessary for calculating the simulated FTIR spectrum, is achieved from the MD simulation by averaging 500 adjacent pieces of the trajectory each containing a 20 ps time window.

2. The vibrational dynamics

Due to the dynamics of the carboxylate sites and solvent molecules in the hydration shell, the vibrational Hamiltonian of the system is time dependent (Eq. (2)). The solution of this particular time-dependent Hamiltonian leads to a system of differential equations of the form

$$\begin{aligned} i\frac{dc_1}{dt} &= \omega_1'(t)c_1 + \beta(t)c_2, \\ i\frac{dc_2}{dt} &= \omega_2'(t)c_2 + \beta(t)c_1, \end{aligned} \tag{10}$$

where c's are the coefficients of the vibrational wave functions in the site basis set. The system of differential equations obtained from the time-dependent Schrödinger equation was solved with a standard algorithm for the instantaneous frequencies and couplings calculated from the MD simulation. The coefficients provide the instantaneous populations of the sites and the instantaneous interstate coherences.[24] To compute observables, the statistical density matrix must be computed by averaging the instantaneous values $c_m^*(t)c_n(t)$ over trajectories describing the ensemble. Such a procedure yields the statistical density matrix

$$\rho_{nm}(t) = \langle c_m^*(t)c_n(t)\rangle. \tag{11}$$

This density matrix allows us to calculate mean values of properties at the temperature of the simulation from traces of system operators over the density matrix (Eq. (11)). Since the MD simulation only produces the time evolution of a single system, the average required for computing the statistical density matrix for values of $t < 10$ ps, was produced by averaging 5000 different 10 ps time windows of the trajectory. A similar scheme was used to calculate the population probabilities for excitonic states. However, for this calculation the coefficients in Eq. (10) are substituted according to their definition (Eq. (3)).

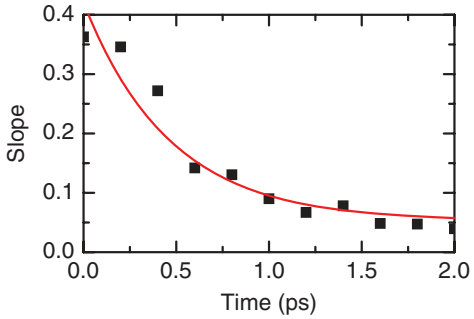

FIG. 7. Slope S(T) versus population time for oxalate (filled squares). The smooth lines are the fits corresponding to Eq. (12) using the parameters given in the text.

B. Frequency-frequency correlation function [FFCF]

The correlations of the frequency fluctuations for the asymmetric stretch are manifested in the 2D IR spectrum.[25] One of the spectral components that contains information about the correlation time is the slope of the zero contour (nodal) line that separates the positive $v = 1 \rightarrow 0$ and negative $v = 1 \rightarrow 2$ transitions. To characterize its dynamics, the slope is measured at the point of intersection with the line joining the peaks for different waiting times, T. The slope versus waiting time for the central transition is presented in Figure 7. The time evolution of this slope suggests a model function of the form

$$S(T) = a_1 \exp(-T/\tau_1) + a_2. \tag{12}$$

The components of the slope dynamics are found to be a decay time of 465 fs with amplitude of $a_1 = 0.35$, and a constant amplitude $a_2 = 0.05$. The experimental slope for the oxalate central transition yields an intercept starting below 0.4. The low value of the intercept indicates that significant correlation is lost too quickly to appear in the slope measurement. The dephasing processes of the oxalate's asymmetric stretch transition have an important contribution from homogeneous processes which include the fast T_1 observed for this transition (see below). In addition, the time evolution of the slope shows two components with completely different time scales: a subpicosecond exponential decay of 0.47 ps and a constant component which does not decay significantly within the observed waiting times of the experiment.

According to the proposed theoretical model, oxalate presents two possible mechanisms for producing a loss of the phase correlation among the oscillators in the ensemble. These are fluctuations in the dihedral angle, and the hydration shell movements. Although the latter may involve only slight dihedral angle changes, they nevertheless cause the carboxylate transition frequencies to fluctuate significantly. The conformation of the ion fluctuates around a mean configuration that has an angle of 90° between the transition dipole moments of each asymmetric stretches (Figure 1). During some periods, the conformation has a dihedral angle well removed

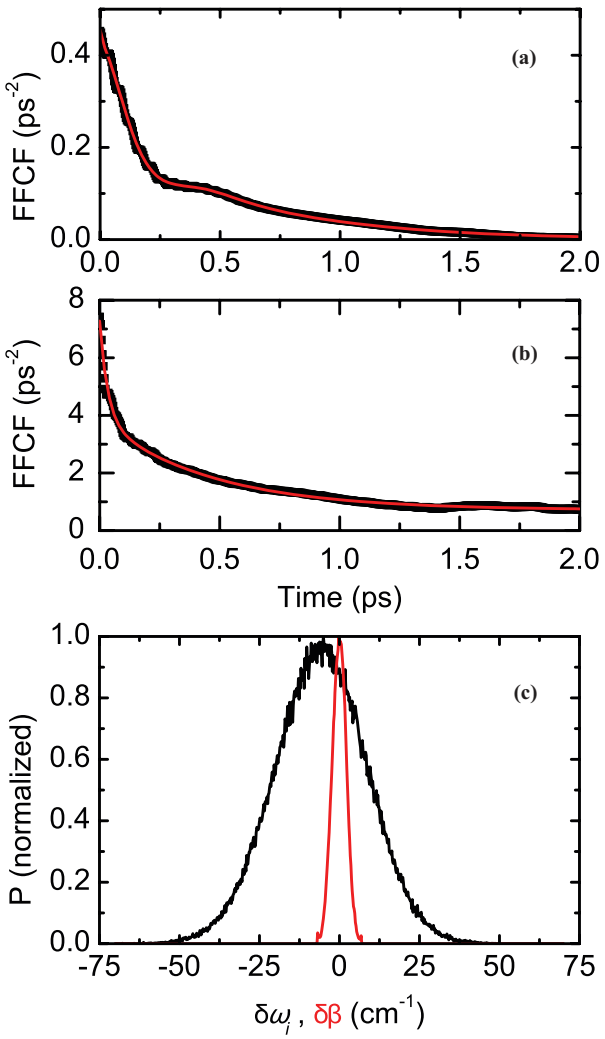

FIG. 8. Autocorrelation of the frequency fluctuations for different mechanisms, and the normalized distribution of their fluctuations. Time correlation function considering (a) only coupling between states and (b) pure solvation dynamics. Filled squares are the FFCF and the solid line is the fit of the correlation function with function given in the text. (c) Distribution function of the frequency fluctuations due to coupling (red line) and solvation dynamics (black line).

from 90° at which point a splitting of the degeneracy of the $v = 1$ state will occur. The mean value of the coupling is zero since $\langle\theta\rangle = 90°$ and $\langle\beta(t)\rangle \propto \langle\cos\theta\rangle$, and the variance in these properties, while significant, is small when compared to the site fluctuation due to solvent rearrangements (Figure 8(c)). Therefore, a change in the coupling between the sites will not make a large contribution to a dephasing process.

The second process that can produce spectral diffusion is the hydration shell dynamics. In this case, the frequency fluctuations are caused by solvent rearrangement within the solvation shell of each carboxylate. As shown in Figures 8(b) and 8(c), the FFCF modeled with solvent fluctuations from the MD simulation predicts a fast dynamics component, a slow dynamic component, and a constant. The fast component has a decay time of 0.03 ps and amplitude of 3.4 ps^{-2}. The intermediate component presents a decay time of 0.46 ps and amplitude of 3.1 ps^{-2}. The third component is a constant on the time scale of the simulation with a value of 0.7 ps^{-2}. Out of these three components, only one is predicted to be observed in the decay of the slope, namely, the intermediate decay, since the fast process is in the homogenous limit, i.e., $\Delta\tau \ll 1$, and the slowest component would stay constant within the longest time measured on the experiment and not cause the slope to decrease. The time scale of the intermediate inhomogeneous process predicted by the frequency fluctuation due to solvent reorganizations is similar to that observed in the experimental slope dynamics. It is concluded by comparisons of the effects of dihedral angle changes and frequency fluctuations from solvent that the hydration shell dynamics is the main process contributing to the experimental slope. Although the time scale of the fast inhomogeneous process in FFCF is one of the fastest ever observed experimentally, it is similar to that observed for another carboxylate.[5]

C. Anisotropy decay and vibrational dynamics

There are a number of possible contributions to the fast decay of the anisotropy shown in Figure 3(b). The first and the most obvious process to consider is orientational diffusion. The MD simulation shows that the dipole reorientation time for a dipole localized in one of the carboxylates has a decay time of ~2 ps which is five times slower than the measured anisotropy decay.[22] A simple calculation based on the Stokes-Einstein-Debye relation gives $1/(6D) \simeq 4.5$ ps.[26] We conclude that rotational diffusion is slow compared with the subpicosecond decay seen in the pump probe anisotropy experiment. The second possible source of the fast decay in the anisotropy arises from solvent induced transfers of excitation between two carboxylate asymmetric stretch modes. The third possibility is that the anisotropy measures the decay of the intersite coherences created by the excitation pulses. Clearly a full description of this system requires some knowledge of the comparative time scales and magnitudes of the coupling and frequency fluctuations of the carboxylate antisymmetric stretch modes.

The thermally averaged coupling between the site states has an rms value of 0.7 cm^{-1} based on the formulation for the coupling given above. The coherence evolution period based on such a coupling is ~50 ps. This estimate takes into account that oxalate is frequently thermally excited to conformations in which the coupling constant is much larger than the standard deviation, for example, it is 10 cm^{-1} at 45°. In any event, the computation indicates that the delocalization in any conformation will be rapidly localized by fluctuations of the solvent. Since energy transfer between the *sites* is much too slow to account for the anisotropy decay, a model incorporating fast energy transfer between the two *delocalized* carboxylate states, $|+(t)\rangle$ and $|-(t)\rangle$, that are prepared by the pulses is used to described the time dependence of the anisotropy.

To derive this model, it is assumed that the transition dipoles for the two sites are of equal length. If the $|+\rangle$ or the $|-\rangle$ state is pumped, the excited system will equilibrate by virtue of the large amplitude, fast frequency fluctuations of the $v = 0 \rightarrow 1$ transitions of the sites. Therefore, the simplest anisotropy model involves contributions from molecules that did and those that did not undergo transfer between the exciton states prior to the arrival of the probe pulse. Such

a model in the absence of the transition dipole magnitude fluctuations yields an anisotropy of $1/2\,(0.4 + 0.4P_2\,(\cos\theta))$ which in the case of perpendicular dipoles gives the average of 0.4 and −0.2 which is 0.1, the anisotropy of a circular oscillator.[27,28]

In the present case, the ZZXX tensor component of the polarized signal at some instant t is, therefore, proportional to

$$I_{zx}(t) = \left\langle P_{++}(t)\mu_{0+}^2(0)\mu_{0+}^2(t)Z_+^2(0)X_+^2(t) + P_{+-}(t)\mu_{0+}^2(0)\mu_{0-}^2(t)Z_+^2(0)X_-^2(t)\right\rangle, \quad (13)$$

where $P_{++}(t)$ is the probability that if a molecule is pumped to a $|+\rangle$ state, then it will be in a $|+\rangle$ state after time t, and $P_{+-}(t)$ is the probability that it has transferred to state $|-\rangle$. The angle brackets imply an average over both the orientations of the transition dipoles with respect to the laboratory axes and the distribution of the dihedral angles. The remaining factor in each term is the magnitude of the signal from that particular diagram. This term strongly depends on the time variation of the magnitudes due to fluctuations in the dihedral angle. The projection of the laboratory Z axis onto the dipole of the $0 \rightarrow |\pm\rangle$ transitions is indicated as $Z_\pm^2(t)$. The kinetics of population transfer between the exciton states is represented by the conditional kinetic factors

$$\begin{aligned} P_{++}(t) &= 1/2(1 + e^{-kt}), \\ P_{+-}(t) &= 1/2(1 - e^{-kt}). \end{aligned} \quad (14)$$

By completing the orientation averages, separating the internal dihedral angle motion from the overall motion, and averaging over the ensemble created by the potential of mean force, the anisotropy becomes

$$r(t) = \frac{I_{ZZ} - I_{ZX}}{I_{ZZ} + 2I_{ZX}} = e^{-6Dt}\,\frac{\left\{0.4\left\langle\mu_{0+}^2(0)\mu_{0+}^2(t)\right\rangle_\theta P_{++}(t) - 0.2\left\langle\mu_{0+}^2(0)\mu_{0-}^2(t)\right\rangle_\theta P_{+-}(t)\right\}}{\left\{\left\langle\mu_{0+}^2(0)\mu_{0+}^2(t)\right\rangle_\theta P_{++}(t) + \left\langle\mu_{0+}^2(0)\mu_{0-}^2(t)\right\rangle_\theta P_{+-}(t)\right\}}. \quad (15)$$

This equation is deduced by averaging over the laboratory axes for a fixed value of the internal angle, followed by a symbolic average over the dihedral angle.[22] The factor of −0.2 arises from the angle between the *plus* and *minus* state transition dipoles being at all times 90°. The $\langle ...\rangle_\theta$ represents the average over the thermal distribution of transition dipole magnitudes which are directly related to the dihedral angles through Eq. (4). Assuming $D = 0$, were it not for the transition dipole magnitudes that vary with fluctuations in the dihedral angle, the anisotropy would decay from 0.4 to 0.1 with time constant $1/k$. This result also comes directly from adding all Liouville path diagrams (see Figure 4 of Ref. 6 for another example) that contribute to the pump-probe signal where a pair of states is undergoing equilibration. The result incorporates a main assumption that the off-diagonal anharmonicity is zero, such that the combination band of the two exciton transitions exactly equals twice the fundamental frequency: this completely eliminates the contributions of the coherent excitations of exciton states from the signal. Also to cancel these diagrams, it is required that the fluctuations in the exciton frequencies are negligible, which is consistent with the model result of there being only small coupling fluctuations. The most important features of this model are first that when population exchange exists between $|+\rangle$ and $|-\rangle$, a fast drop in the anisotropy will be observed regardless of any orientational dynamics. Furthermore, the fluctuations in frequency of the site states must be responsible for the decay of the anisotropy because the coupling between the two carboxylates is very small. Introducing the results from Eq. (4) leads to an anisotropy

$$r(t) = e^{-6Dt}\,\frac{0.4P_{++}(t) - 0.2\alpha P_{+-}(t)}{P_{++}(t) + \alpha P_{+-}(t)}, \quad (16)$$

where the parameter α that depends on the dihedral angle potential function and the temperature is given by

$$\alpha = \frac{1 - \langle\cos\theta(0)\cos\theta(t)\rangle_\theta}{1 + \langle\cos\theta(0)\cos\theta(t)\rangle_\theta}, \quad (17)$$

where $\theta(t)$ is the dihedral angle reached by time t after excitation at an angle $\theta(0)$. This α parameter varies from 0 to 1 limiting the second term of Eq. (16) to values from 0.1 to 0.4. According to the MD simulation, correlations of $\cos\theta$ have the same time dependence as those of $\beta(t)$ (Figure 8(a)). The variance in $\cos\theta$ is $\langle\cos^2\theta\rangle_\theta = 0.11$, so the factor begins at 0.80 and reaches a unity on a 100 fs time scale. Because $\rho_{+-}(t) = 0$ at $t = 0$ and only grows with a rate defined by population transfer, $k = 1/(500\text{ fs})$, the effect of α on the anisotropy is negligible. If indeed the anisotropy plateaus higher than 0.1, as indicated by the very noisy experimental result, then α would be required to decay much more slowly than predicted by the MD simulation, which predicts a value of 0.1 for very slow overall motion. Therefore, the associated water may be impeding the changes in dihedral angle to a greater extent than is simulated. Future directions involve a closer evaluation of the coupling between internal and overall motion of the ion.

The proposed anisotropy model distinguishes between whether the system is initially excited to a localized or a delocalized state. It provides an interpretation of the time dependence of the anisotropy in terms of the population transfer between exciton states which is equivalent to the loss of the coherences between the sites due to their frequency fluctuations. In other words, the anisotropy decay tracks the localization of the oxalate delocalized vibrational excitation onto one carboxylate or the other. This interpretation is fully supported by the calculations based on the MD simulation which show that the coupling fluctuations are very small compared with those of the site vibrational frequency. The rate of population

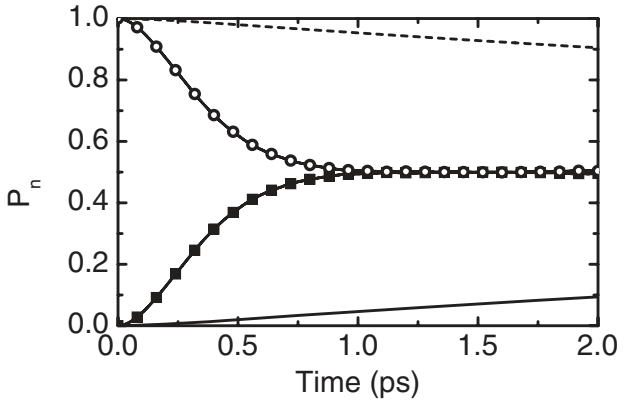

FIG. 9. Time dependence of the population P_n. Dashed and solid lines represent the time evolution of the site populations. Squares and circles show the time dependence of the populations of the $|+\rangle$ and $|-\rangle$ exciton states. In both cases the system is initially prepared by preparing the population in a pure site or exciton state.

transfer between the two $v = 1$ states of the ion was obtained from the time-dependent Schrödinger equation as described above. The system at $t = 0$ was started out in a pure site or pure exciton state. Figure 9 shows the time evolution of the site and exciton populations from the diagonal elements of the density matrix. While the population transfer from a system initially localized at one site shows a decay time of the initially populated state of ~20 ps (Figure 9), the system initially prepared in a pure exciton state decays with a rate constant of ~0.3 ps. The difference in the population dynamics is indicative of a system highly perturbed by the solvent fluctuations of the vibrational frequency and only slightly perturbed by coupling between the site states. The coupling term in the Hamiltonian ($\beta(t)$) is the main contributing factor for delocalizing the initially localized site state, and the much larger site fluctuations ($\delta\omega_i(t)$) are responsible for localizing the delocalized exciton state. The localization of the delocalized states is also observed in the theory as a corresponding ultrafast decay of the elements, $\rho_{12}(t)$, of the site density matrix.

In the case of initially preparing a pure site state, the anisotropy would be defined by the restricted dipole reorientation of this site, but according to the MD simulation, the population transfer itself is not sufficiently fast to produce the observed decay. Nevertheless the molecule quickly moves from this configuration. In contrast, the population transfer between excitonic states is controlled by large, ultrafast site fluctuations. For the system initially prepared in a pure exciton state, the calculated rate of exchange between $|+\rangle$ and $|-\rangle$ states is ~0.3 ps which is close to the decay time of the anisotropy (0.4 ps). Therefore, comparing the anisotropy decay with theory suggests that a microscopic picture of the dipole reorientation where there are 90° flips of the transition dipole caused by solvent induced population transfer between the *plus* and *minus* delocalized states in the ensemble of dihedral angles. The off diagonal elements of the site density matrix decay on this same time scale as a result of the site vibrational frequency fluctuations. At this stage we have not eliminated the possible role of indirect energy transfer between the carboxylate groups through the intermediacy of other delocalized modes of the oxalate ion such have been reported for other more complex molecules.[32]

Our Hamiltonian is equivalent to other two level calculations such as in Refs. 23, 28, and 29. However, our approach is entirely numerical based on a simulation following the approach of Ref. 24. We have not compared our numerical results to those obtained from the analytic formulas, given in Refs. 23, 28, and 29, in terms of correlation and cross correlation functions of frequency and coupling, although they could be estimated from the MD simulation. This question will be addressed in future work.

D. Population, T_1, relaxation of the aqueous oxalate dianion

Oxalate manifests a population relaxation of the $v = 1$ antisymmetric stretching modes, which is well described by a biexponential decay. This same type of population relaxation was previously observed for the trifluoroacetate ion and was attributed to a mechanism in which there is solvent induced transfer between the asymmetric and the symmetric stretch modes.[5] The kinetics linking the asymmetric and symmetric stretches is modeled by a bidirectional mechanism satisfying microscopic reversibility such that the passage from the asymmetric to the symmetric stretch is $\exp[\Delta E/k_bT]$ times the back transfer, where ΔE is the energy difference between the two states. It has been proposed that this mode coupling mechanism is a general property of carboxylates.[5] The population relaxation of oxalate supports this idea. When the simplified kinetic scheme that describes carboxylate excited state populations is applied to the oxalate pump-probe signal at the location of the excited state absorption, the following rate coefficients are obtained: $k_{AS} = 1.55\,\text{ps}^{-1}$, $k_{SA} = 0.99\,\text{ps}^{-1}$, $k_{A0} = 0.98\,\text{ps}^{-1}$, and $k_{S0} = 0.45\,\text{ps}^{-1}$. The frequency difference between the asymmetric and symmetric modes computed from the rate coefficients k_{AS} and k_{SA} is 92 cm^{-1}.

In oxalate, the asymmetric stretch of each site should be coupled with its own symmetric stretch. The highest frequency mode of the symmetric stretch is at 1490 cm^{-1} which corresponds to the out of phase symmetric stretch (Figure 1).[8] This mode is 89 cm^{-1} below the asymmetric stretch of oxalate which is very close to the gap measured by the kinetics of the populations. These results suggest that oxalate, like TFA,[5] has a population relaxation mechanism that involves a solvent-assisted equilibration between the symmetric and asymmetric stretches. A precise knowledge of the pathways of relaxation between the various linear combinations of carboxylate states formed by the two sites is not made evident by these results and needs further work.

E. Linear infrared spectrum

The linear absorption spectrum $S(\omega)$ of oxalate is modeled according to Eq. (9). Oxalate's asymmetric stretch line shape is the convolution of three different processes: lifetime of the excited state, coupling between carboxylate sites, and fluctuation of the sites frequencies due to solvent reorganizations.

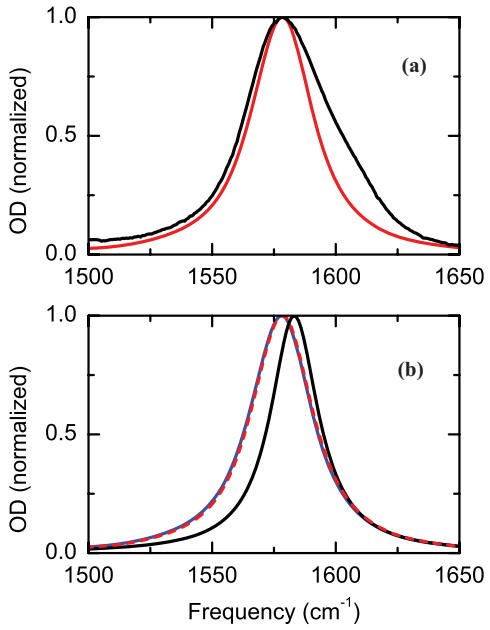

FIG. 10. Linear IR spectra of oxalate. (a) The black line is the experimental absorption line shape and the red line is predicted one as discussed in the text relating to Eq. (9). (b) Modeled FTIR spectrum with different component in the FFCF: only lifetime (black line), lifetime and fluctuations in dihedral angle and hydration shell dynamics (dash red line), and lifetime, transition dipole, and fluctuations in dihedral angle and hydration shell dynamics (blue line).

Figure 10 shows the different linear spectra obtained when different components are included in the model. If the T_1 lifetime of excited state is considered, the linear spectrum shows the expected Lorentzian shape and a full width at half maximum of 24 cm^{-1}. Incorporation of the coupling between sites to the previous model produces a line shape where no additional broadening is observed. The next process accounted for modeling the linear absorption spectrum is the fluctuations of the frequency, $\delta\omega_i$, due to solvent dynamics. As observed in Figure 10, the predicted absorption band is not only significantly broader than when the lifetime of the transition is solely considered (broadens by 7 cm^{-1}), but also has a shift of 5 cm^{-1} in the central frequency. This redshift is consistent with the stabilization of the carboxylate asymmetric stretch by hydrogen bonding to water.[30] The last process incorporated into the linear absorption spectrum is the fluctuation of the transition dipole, $\mu_i(t)$, due to coupling. Although the effect is not large, a detailed inspection of the modeled line shape reveals that the asymmetric stretch absorption band becomes slightly asymmetric (skewness parameter of 0.025). The asymmetry on the line shape is produced by the time dependence of the transition dipole magnitude fluctuation.[31] In the coupled basis set, the state with the higher transition frequency always has a transition dipole moment magnitude that is larger than the lower one on both sides of $\theta_{ab} = \pi/2$ in the potential well. This condition arises because the coupling changes sign as the dihedral angle passes through $\pi/2$. Thus, the coupling process creates a dependence of the transition dipole moment on the frequency which results in an asymmetry in the line shape in the linear absorption. The small effect of the magnitude of the transition dipole magnitude on the line shape agrees well with the ion only exploring a very small part of the potential energy surface close to the minimum of energy at 90° where the coupling is very small and where the fluctuation of the transition dipole magnitude is correspondingly small (Figure 8(c)).

There is a good agreement between the predicted and the experimental linear infrared spectra. However, one important difference between the predicted and the experimental infrared spectrum is the shoulder located on the higher frequency edge of the band. This shoulder, also observed in the 2D-IR spectrum as a peak at 1608 cm^{-1}, corresponds to the asymmetric stretch transition of oxalate forming an ion pair.

V. CONCLUSION

Ultrafast vibrational spectra of the aqueous oxalate ion in the region of its carboxylate asymmetric stretch modes show novel relaxation processes. Two-dimensional infrared vibrational echo spectra and the vibrational dynamics obtained from them along with measurements of the anisotropy decay provide a picture in which the localization of the oxalate vibrational excitation onto the carboxylate groups occurs in ~450 fs. The localization results from the water induced fluctuations in the carboxylate vibrational frequencies which are shown to have a similar correlation time. The experiments are supplemented by a calculation of the potential of mean force for rotation of the dihedral angle between the two carboxylate planes and MD simulations of the motion of the ion on this potential. The ion has a mean dihedral angle of $\pi/2$ corresponding to D_{2d} symmetry where the asymmetric stretch mode is degenerate. Although the dihedral angle motions cause significant fluctuations in the splitting between the $v = 1$ vibrational states that cause a noticeable asymmetry in the infrared spectrum, the hydrogen bond dynamics with water molecules in the first solvent shell dominates the vibrational dynamics.

ACKNOWLEDGMENTS

We thank Professor Gerhard Stock and Professor Cyril Falvo for helpful discussions. This research was supported by grants from the NSF-CHE and the NIH-GM12592 with instrumentation supported by NIH-RR001348.

[1] P. Ball, Chem. Rev. **108**, 74 (2008).
[2] K. J. Tielrooij, N. Garcia-Araez, M. Bonn, and H. J. Bakker, Science **328**, 1006 (2010).
[3] S. Park, M. Odelius, and K. J. Gaffney, J. Phys. Chem. B **113**, 7825 (2009).
[4] C. H. Kuo, D. Y. Vorobyev, J. X. Chen, and R. M. Hochstrasser, J. Phys. Chem. B **111**, 14028 (2007).
[5] D. G. Kuroda, D. Y. Vorobyev, and R. M. Hochstrasser, J. Chem. Phys. **132**, 044501 (2010).
[6] D. Y. Vorobyev, C. H. Kuo, J. X. Chen, D. G. Kuroda, J. N. Scott, J. M. Vanderkooi, and R. M. Hochstrasser, J. Phys. Chem. B **113**, 15382 (2009).
[7] D. Y. Vorobyev, C. H. Kuo, D. G. Kuroda, J. N. Scott, J. M. Vanderkooi, and R. M. Hochstrasser, J. Phys. Chem. B **114**, 2944 (2010).
[8] R. J. H. Clark and S. Firth, Spectrochim. Acta, Part A **58**, 1731 (2002).
[9] A. R. Hind, S. K. Bhargava, W. Van Bronswijk, S. C. Grocott, and S. L. Eyer, Appl. Spectrosc. **52**, 683 (1998).
[10] G. M. Begun and W. H. Fletcher, Spectrochim. Acta **19**, 1343 (1963).
[11] R. L. Frost and M. L. Weier, J Raman Spectrosc **34**, 776 (2003).
[12] J. M. Herbert and J. V. Ortiz, J. Phys. Chem. A **104**, 11786 (2000).
[13] A. Ghosh, M. J. Tucker, and R. M. Hochstrasser, J. Phys. Chem. A **115**, 9731 (2011).

[14]A. Remorino, I. V. Korendovych, Y. B. Wu, W. F. DeGrado, and R. M. Hochstrasser, Science **332**, 1206 (2011).
[15]A. Ghosh, J. Qiu, W. F. DeGrado, and R. M. Hochstrasser, Proc. Natl. Acad. Sci. U.S.A. **108**, 6115 (2011).
[16]M. J. Tucker, X. S. Gai, E. E. Fenlon, S. H. Brewer, and R. M. Hochstrasser, Phys. Chem. Chem. Phys. **13**, 2237 (2011).
[17]Y. S. Kim, J. P. Wang, and R. M. Hochstrasser, J. Phys. Chem. B **109**, 7511 (2005).
[18]D. A. Case, T. A. Darden, T. E. I. Cheatham, C. L. Simmerling, J. Wang, R. E. Duke, R. Luo, K. M. Merz, D. A. Pearlman, M. Crowley, R. C. Walker, W. Zhang, B. Wang, S. Hayik, A. Roitberg, G. Seabra, K. F. Wong, F. Paesani, X. Wu, S. Brozell, V. Tsui, H. Gohlke, L. Yang, C. Tan, J. Mongan, V. Hornak, G. Cui, P. Beroza, D. H. Mathews, C. Schafmeister, W. S. Ross, and P. A. Kollman, *AMBER 9*, 9th ed. (University of California, San Francisco, 2006).
[19]A. Grossfield, "WHAM: the weighted histogram analysis method," version 2.0.4, http://membrane.urmc.rochester.edu/content/wham.
[20]S. Bagchi, C. Falvo, S. Mukamel, and R. M. Hochstrasser, J. Phys. Chem. B **113**, 11260 (2009).
[21]G. Hefter, Pure Appl. Chem. **78**, 1571 (2006).
[22]See supplementary material at http://dx.doi.org/10.1063/1.3658461 for comparison between photo induced absorption and bleach signal dynamics; transition dipole autocorrelation function; and derivation of Eq. (15).
[23]R. Wertheimer and R. Silbey, Chem. Phys. Lett. **75**, 243 (1980).
[24]M. Kobus, P. H. Nguyen, and G. Stock, J. Chem. Phys. **134**, 124518 (2011).
[25]P. Hamm, M. Lim, and R. M. Hochstrasser, Phys. Rev. Lett. **81**, 5326 (1998).
[26]M. Lee, A. J. Bain, P. J. Mccarthy, C. H. Han, J. N. Haseltine, A. B. Smith, and R. M. Hochstrasser, J. Chem. Phys. **85**, 4341 (1986).
[27]A. Szabo, J. Chem. Phys. **81**, 150 (1984).
[28]K. Wynne and R. M. Hochstrasser, J. Raman Spectrosc. **26**, 561 (1995).
[29]H. Haken and G. Strobl, Z. Phys. **262**, 135 (1973).
[30]A. K. Dioumaev and M. S. Braiman, J. Am. Chem. Soc. **117**, 10572 (1995).
[31]S. A. Corcelli and J. L. Skinner, J. Phys. Chem. A **109**, 6154 (2005).
[32]I. V. Rubtsov, Acc. Chem. Res. **42**, 1385 (2009).